Long-fiber Embedded Hydrogel 3D Printing for Structural Reinforcement

Wenhuan Sun,[†] Joshua W. Tashman,[‡] Daniel J. Shiwarski,[‡] Adam W. Feinberg,[‡,¶] and Victoria A. Webster-Wood[*,†,‡]

†*Department of Mechanical Engineering, Carnegie Mellon University, Pittsburgh, PA 15213, USA*

‡*Department of Biomedical Engineering, Carnegie Mellon University, Pittsburgh, PA 15213, USA*

¶*Department of Materials Science & Engineering, Carnegie Mellon University, Pittsburgh, PA 15213, USA*

E-mail: vwebster@andrew.cmu.edu

Phone: +1 412.268.3017

Abstract

Hydrogels are candidate building blocks in a wide range of biomaterial applications including soft and biohybrid robotics, microfluidics, and tissue engineering. Recent advances in embedded 3D printing have broadened the design space accessible with hydrogel additive manufacturing. Specifically, the Freeform Reversible Embedding of Suspended Hydrogels (FRESH) technique has enabled the fabrication of complex 3D structures using extremely soft hydrogels, e.g., alginate and collagen, by assembling hydrogels within a fugitive support bath. However, the low structural rigidity of FRESH printed hydrogels limits their applications, especially those that require operation in non-aqueous environments. In this study, we demonstrated long-fiber embedded hydrogel 3D printing using a multi-head printing platform consisting of a custom-built

fiber extruder and an open-source FRESH bioprinter with high embedding fidelity. Using this process, fibers were embedded in 3D printed hydrogel components to achieve significant structural reinforcement (e.g., tensile modulus improved from 56.78 ± 8.76 kPa to 382.55 ± 25.29 kPa, tensile strength improved from 9.44 ± 2.28 kPa to 45.05 ± 5.53 kPa). In addition, we demonstrated the versatility of this technique by using fibers of a wide range of sizes and material types and implementing different 2D and 3D embedding patterns, such as embedding a conical helix using electrochemically aligned collagen fiber via non-planar printing. Moreover, the technique was implemented using low-cost material and is compatible with open-source software and hardware, which facilitates its adoption and modification for new research applications.

Keywords: Fiber embedding, FRESH printing, multi-material printing, hydrogel

Introduction

Hydrogels are porous and hydrophilic networks of crosslinked polymers with a wide range of benefits including bio-compatibility and variable material properties based on chemical composition and fabrication process.[1] In addition, some types of hydrogels have shown stimuli-responsive properties, such as humidity dependent swelling, enabling controlled actuation upon changing environmental cues. Such properties have placed hydrogels as candidate materials for numerous applications, including tissue engineering,[2] drug delivery,[3] microfluidics,[4] and soft and biohybrid robotics.[5] Compared with traditional methods for 3D hydrogel structure fabrication, such as die-casting and electrospinning, hydrogel 3D printing greatly expands the geometric design space that can be fabricated. Several 3D printing strategies have been introduced to create functional hydrogel components,[6] including inkjet printing,[7] laser-based printing such as two-photon polymerization (2PP),[8–10] stereolithography (SLA),[11,12] digital light processing (DLP),[13] and extrusion based printing.[14–16]

Despite the success of hydrogel additive manufacturing techniques, 3D printing complex hydrogel structures without support is still challenging because many hydrogel bioinks are

extremely soft and cannot support their own weight during printing. One successful strategy to tackle this issue is to use supportive granular media that fluidizes upon shear stress from needle movement and quickly solidifies to trap newly deposited hydrogels in place during printing and subsequent crosslinking.[17] This type of granular gel medium overcomes the challenges of surface tension, gravity, and particle diffusion and enables additive manufacturing of complex objects with a large aspect ratio and high resolution using a variety of soft materials.[18–29] A representative granular media-based printing technique is the Freeform Reversible Embedding of Suspended Hydrogels (FRESH),[30] where hydrogel structures are printed in a support bath made of gelatin microparticles that provide support during printing and subsequently liquefy upon raised temperature for part retrieval. Since its inception, FRESH has been applied to fabricate a wide range of functional hydrogel components, including components of the human heart from capillaries to the full organ scale[30,31] and cardiac ventricles printed with human cardiomyocytes showing synchronized contractions.[32]

While advances in granular media based printing techniques,[17,33,34] such as FRESH[31,32], have allowed 3D bioprinting of complex hydrogel components, the low structural rigidity of FRESH printed hydrogel components limits their applications, especially for those require handling or operation in non-aqueous environments where structural reinforcement of FRESH printed hydrogels is needed. To increase material strength, fibers with high strength can be combined with the base material to create fiber reinforced composites, such as fiberglass reinforced plastic. This concept of fiber embedding has been previously applied to cast hydrogels to enable structural reinforcement and additional functions. For example, hydrogel components can be cast with conductive fibers to produce sensors and electrodes,[35,36] or with nanofibers made from electrospinning, bacteria products, and melt electrowriting to enhance mechanical properties.[37–39] However, casting limits the geometries that can be easily fabricated and increases costs for iterative prototyping. 3D printing methods, such as FRESH, provide an alternative fabrication method for creating complex structures with hydrogels. However, fabrication methods or tools to embed continuous and strong fibers into

the hydrogel during printing have not been previously reported.

Here, we report the development of a 3D printing method to embed long-fiber in hydrogels for structural reinforcement in a process termed long-fiber embedding FRESH (LFE-FRESH). To achieve this, we designed a multi-head printing platform consisting of a continuous long-fiber extruder integrated with an extrusion-based FRESH bioprinter for hydrogels. The embedding process requires fibers to be stiff enough to prevent buckling. Therefore, identifying qualified fibers is important for successful embedding. To facilitate fiber material selection, we developed and experimentally validated a design diagram of fiber printability prediction based on fiber properties. LFE-FRESH's high embedding fidelity was confirmed using optical coherence tomography imaging. Fiber-hydrogel boding strength, a critical component of structural reinforcement in composite materials, was measured using fiber pull-out testing on fiber embedded, 3D printed alginate. Additionally, to demonstrate significant structural reinforcement via fiber embedding, tensile testing and three-point bending were performed on 3D printed alginate with and without embedded fibers. Finally, we demonstrated the versatility and potential applications of this technique by implementing a range of 2D and 3D embedding patterns using different fiber types including commercially available sewing threads and custom-made eutectic Gallium Indium-alginate fiber. Together with the open-source nature of this fabrication tool, these results lay the groundwork toward hydrogel 3D printing with long-fiber embedding enabling structural reinforcement and additional functionalities in hydrogel structures.

Materials and methods

Preparation of Alginate, Collagen Ink, and Gelatin Support Bath

The LFE-FRESH technique was tested using several biocompatible inks and support material. In particular, the technique was tested with alginate[40] and collagen ink[32] and a gelatin support bath[30]. Alginate ink for FRESH printing was prepared by solubilizing sodium al-

ginate powder (mannuronic to guluronic acid ratio (M/G) is 1:3, Allevi) in deionized (DI) water to achieve the desired concentration (4% w/v). Optionally, Alcian Blue dye (Alfa Aesar) powder was added to the mixture to achieve 0.02% w/v to facilitate visualization during printing and imaging. A collagen stock solution (6 mg/mL acid soluble collagen in 0.01 N HCl, Collagen Solutions) was used as the collagen ink for FRESH printing without further modification. The gelatin support bath preparation was performed following previously published protocols[31,32] using a complex coacervation method with slight modifications. Briefly, the gelatin precursor solution was made by solubilizing 2.0% w/v gelatin Type B (Fisher Chemical), 0.25% w/v Pluronic F-127 (Sigma-Aldrich), and 1.0% w/v gum arabic (Sigma-Aldrich) in a 50% v/v ethanol solution at 60 ^{0}C in a 2L beaker and adjusted to 6.28-6.30 pH by adding 1N sodium hydroxide (NaOH) (Fisher Chemical) dropwise. The precursor solution was then stirred for 24 hours while cooling to room temperature (21 - 25 ^{o}C) and the resulting gelatin slurry was washed three times with bioink-dependent washing solution (0.1% calcium chloride (CaCl2) for alginate ink, 1x PBS (Gibco) for collagen ink). To form the compacted support bath material for FRESH printing, the slurry was centrifuged at 2000 g for 5 minutes prior to printing.

Preparation of Fibers for Embedding: Electrochemically Aligned Collagen Fiber and Eutectic Gallium Indium-Alginate

Fiber-embedding was performed with three commercially available fibers (polyester, silk fibers (110 yds, Gutermann) and stainless-steel fibers (Adafruit)), and two custom fibers fabricated in house (electrochemically aligned collagen,[41] and eutectic gallium indium-alginate). These fibers were selected to test the LFE-FRESH technique across a wide range of material properties and fiber dimensions. Additionally, silk,[42] polyester,[43] and electrocompacted and aligned collagen threads[44] have good biocompatibility and have been previously used in a wide variety of tissue engineering techniques. Furthermore, eutectic gallium indium has been used in wearable devices and can be encapsulated to ensure biocompatibility.[45–47]

Electrochemically aligned collagen (ELAC) fibers were fabricated following previously reported protocols.[41,48,49] Briefly, the collagen stock solution (6 mg/mL, Collagen Solutions) was diluted to 3 mg/mL and dialyzed for 9 h against DI water at 4-10 ^{o}C. The collagen solution was subsequently deposited between a pair of stainless-steel electrodes (diameter: 0.25 mm, Malin) and subjected to a voltage of 20 VDC to induce isoelectric focusing of collagen, which formed long ELAC fibers (length: 150 - 200 mm). To induce fibrillogenesis and improve structural strength, the ELAC fibers were incubated in 1x PBS at 37 ^{o}C for 5 h followed by crosslinking with 0.625 % w/v genipin (Wako Chemicals) in a 90 % v/v ethanol solution for 24 h. To enhance the optical contrast between embedded ELAC fibers and FRESH printed alginate during optical coherence tomography (OCT) imaging, Titanium dioxide (TiO2) powders were dispersed in collagen solution prior to isoelectric focusing to make TiO2-doped ELAC fibers for the OCT imaging group (0.025% w/v).

Eutectic Gallium Indium-alginate (EGaIn-alginate) fibers used in this study were fabricated by pushing 4 g EGaIn (Gallium Source) and 10 mL of 4% w/v sodium alginate solution back and forth between two mated syringes 50 times and extruding the mixture into a 1% CaCl2 solution for crosslinking.

Long-fiber Embedded Hydrogel 3D Printing Process

To perform the LFE-FRESH process, we designed an integrated multi-head printing platform using a custom-designed continuous fiber extruder and a previously reported open-source 3D bioprinter[32] with slight modifications (Fig. 1A). Briefly, the fiber extruder feeds a section of fiber through a set of two guiding tubes using a pair of compliant silicone wheels, which are gear-driven by a Nema 17 stepper motor (Stepperonline). Both the fiber extruder and a Replistruder 3 syringe pump[32] with a G30 needle were mounted onto an open-source, low-cost desktop 3D printer (Creator Pro, FlashForge), replacing the original fused deposition modeling extruder.

Geometric codes (G-code), a programming language for computer numeric control, in

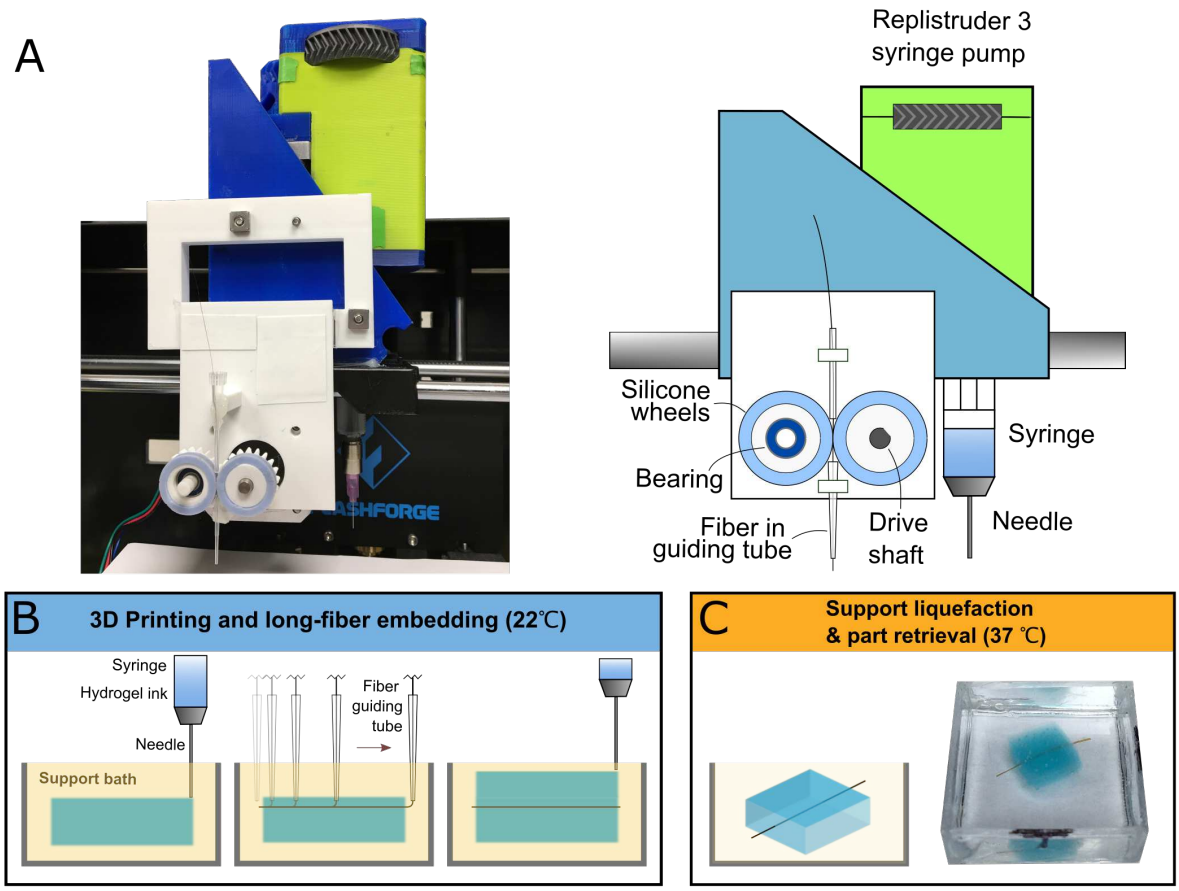

Figure 1: Long-fiber embedded hydrogel 3D printing (LFE-FRESH) is performed using a multi-head printing platform. (A) A photo (left) of the multi-head printing platform, where the fiber extruder and Replistruder 3 syringe pump are mounted onto the carriage of an open-source desktop 3D printer, replacing the original FDM extruder, and a schematic drawing (right) showing a zoom-in view of the extruders (B) A schematic drawing of the LFE-FRESH process (left). A first layer of hydrogel was printed into the support bath, the long-fiber is embedded in the hydrogel, and a second layer of hydrogel is printed to encapsulate the thread. (C) The support bath material liquefies upon raised temperature (right), enabling part retrieval, as shown in the photo of a long-fiber embedded, 3D printed hydrogel floating in the printing container

this study were generated using a combination of closed- and open-source softwares and custom Python scripts. For FRESH printing of hydrogels, all digital models were created using Solidworks 2019 (Dassault Systèmes), exported as STL format files, and converted to G-code using Slic3r (`http://slic3r.org`) with 20 mm/s print speed, 80 μm layer height and using all perimeters with no infill pattern in general (exceptions were the alginate components in Fig. 6K, M, O-Q that were printed with 25% infill density). For 2D long-fiber embedding, the embedding paths were created using Solidworks, exported as DXF format files, modified using LibreCAD to remove unwanted features such as auxiliary lines in the drawing (`https://librecad.org/`) and converted to a preliminary G-code (motion control only without fiber extruder control) using DXF2GCODE (`https://sourceforge.net/projects/dxf2gcode/`). The preliminary G-code was subsequently processed using a custom Python script to add the fiber extruder control commands. For 3D long-fiber embedding, the embedding paths were created and converted to G-code using custom Python scripts. Instructions on using the Python scripts can be found in the Supporting Information of this manuscript.

A typical long-fiber embedded printing process is a combination of hydrogel 3D printing and fiber embedding as illustrated in Fig. 1B. Prior to printing, hydrogel ink was transferred into a gas-tight glass syringe, which was loaded into the Replistruder 3. Compacted gelatin support bath material was transferred into a clear plastic container for printing. The needle was manually positioned to the desired start point and the FRESH printing of the first hydrogel layer was subsequently started by sending G-code to the bioprinter using ReplicatorG (`http://replicat.org/`). Upon completion of the first hydrogel layer, a section of long-fiber was loaded into the fiber extruder and manually positioned to the desired start point (1 mm into the hydrogel layer). Fiber embedding was performed using ReplicatorG and, at the end of the print path, the embedded fiber was manually cut from the stock fiber at the guiding tube. After fiber embedding, the second layer of hydrogel was FRESH printed onto the previously printed hydrogel with a 500 μm Z-height overlap into the first hydrogel layer

to ensure proper bonding. The printing container was subsequently placed into a container filled with 0.1% w/v CaCl2 solution and incubated in a 37 ^{o}C water bath allowing the gelatin slurry to gradually liquefy. The fiber embedded FRESH printed hydrogel was then retrieved and washed with a 0.1% w/v CaCl2 solution. For fiber embedding of non-planar features, the printing process consists of only the 3D printing of the first hydrogel layer and fiber embedding. Briefly, after printing the hydrogel structure, the fiber extruder was manually positioned to the desired start point and instructed to perform 3D fiber embedding where the fiber extruder moves simultaneously in the X, Y, and Z axes. ELAC fibers were used for long-fiber embedding in this work unless specified otherwise. Detailed fiber composition in each embedding can be found in the captions of Fig. 3-6.

Fiber Printability Analysis

During embedding, the fiber is subject to compression load and prone to buckling due to the high slenderness ratio ($\geq$200). Therefore, it is important to maintain fiber stability during embedding by identifying minimum requirements for candidate fibers. To study the geometric and material property constraints to prevent fiber buckling, the fiber section in the lower guiding tube was modeled as a slender column with a circular cross-section under compression with fixed-fixed ends. Using Euler's critical load equation, the critical buckling force or the minimal compression load to initiate fiber buckling, P_{cr} can be expressed as:

$$P_{\text{cr}} = \frac{\pi^2 E_{\text{fiber}} I_{\text{fiber}}}{(KL)^2} \tag{1}$$

where $L = 24$ mm is the unsupported length of the fiber, $K = 0.65$ is the recommended effective length factor for fixed-fixed ends, E_{fiber} is the Young's modulus of the fiber, $I = \frac{\pi d^4}{64}$ is the area moment of inertia of fiber cross section, given circular cross section with fiber diameter d. Meanwhile, the load that is required to push the fiber into FRESH printed bioink can be expressed as $F_{\text{bioink}} = \sigma_{\text{bioink}} A_{\text{contact}}$, where σ_{bioink} is the yield strength of

FRESH printed bioink and $A_{\text{contact}} = \frac{\pi d^2}{4}$ is the contact area between fiber and bioink. To prevent buckling, we need $P_{\text{cr}} \geq F_{\text{bioink}}$, which can be reorganized as:

$$\frac{E_{\text{fiber}}}{\sigma_{\text{bioink}}} \geq \frac{16K^2L^2}{\pi^2 d^2} \tag{2}$$

Therefore, for any given fabrication scenario, the fiber is considered printable if and only if Inequality 3 is valid, which established fiber printability as a function of fiber diameter d and the ratio between fiber Young's modulus and bioink yield strength $\frac{E_{\text{fiber}}}{\sigma_{\text{bioink}}}$. Subsequently, a design diagram was produced where the green and red regions representing printable and non-printable fiber properties were separated by a theoretical boundary:

$$\frac{E_{\text{fiber}}}{\sigma_{\text{bioink}}} = \frac{16K^2L^2}{\pi^2 d^2} \tag{3}$$

Print Fidelity Assessment using Optical Coherence Tomography (OCT) imaging

To investigate the geometric fidelity of the embedded long-fiber, OCT imaging was performed on an LFE-FRESH printed alginate structure with embedded, S-shaped, and TiO2-doped ELAC fibers.[50] Prior to imaging, the sample was transferred to a petri dish and covered with a 50 mM HEPES 0.1% w/v CaCl2 solution. The sample was then placed under the OCT scan head (Thorlabs Vega VEG210 with OCT-LK4 objective) and its volume was acquired using the Thorlabs OCT acquisition software. The raw image was processed in ImageJ (US National Institute of Health) to isolate voxels representing the embedded TiO2-doped fiber based on a grayscale intensity threshold. The coordinates of the voxels were then exported to MATLAB (R2018b, Mathworks) and compared against the input geometry to quantitatively assess embedding quality in terms of absolute displacement from the input geometry. For qualitative assessment, ImageJ was used to produce 2D projected views and 3D rendering of the sample from the OCT imaging data.

Mechanical Characterization of Printed Structures

Embedded Fiber Pull-out Testing

Bonding strength is a critical component of structural reinforcement in composite materials. To assess the fiber-hydrogel bonding strength following fabrication, pull-out testing was conducted using an electromechanical universal testing system with a Biobath chamber and 50 N load cell (Criterion, MTS). Pull-out testing was performed on 3D printed alginate with embedded U-shaped ELAC fibers with and without chemical crosslinking to further investigate the impact of crosslinking treatments on material properties. Briefly, each sample was fabricated by the aforementioned fiber embedded 3D printing process so that a U-shaped ELAC fiber was partially embedded in the mid-plane of an alginate block (6 × 6 × 4 mm, width × height × thickness). The embedded portion resulted in two parallel embedded fibers and the non-embedded section of the fiber formed a loop for test fixturing. For the baseline group, the samples were incubated in DI water for 24 h at room temperature prior to testing. For the crosslinking group, the samples were incubated in a 1% w/v 1-Ethyl-3-(3-dimethylaminopropyl) carbodiimide (EDC) (Thermo Scientific), 0.25% w/v N-hydroxysulfosuccinimide (NHS) (Thermo Scientific) crosslinking solution for 24 h at room temperature and washed with DI water prior to testing. The EDC+NHS crosslinker reacts alginate with collagen via amide linkage.[51] Each sample was bonded to a plate fixed to the bottom of the Biobath chamber using water-resistant glue (Ultra-Gel Control Super Glue, Locktite). An L-shaped stainless steel pin was connected to the load cell via an extender rod and placed through the non-embedded fiber loop. The pin-fiber contact point was secured using the water-resistant glue. 0.1% CaCl2 solution was then pumped into the Biobath chamber and maintained at a constant level. The pin was subsequently loaded and pulled the embedded fiber out of the samples at a rate of 10 mm/min (N = 3 for each group). To eliminate the influence of flotation force on the extender rod while it was pulled out of the bath, the change in flotation force was calculated using solution density and extender

rod geometry as a function of displacement and subtracted from the load cell reading. The pull-out force was calculated as the maximum tensile force achieved by each sample.

Tensile Testing

Tensile testing was performed on the samples to assess the reinforcement effect of fiber embedding. Alginate blocks (6 × 6 × 4 mm, width × height × thickness) were 3D printed using the aforementioned FRESH printing process. As a control, samples in the baseline group were stored in DI water at room temperature for 24 h. Because crosslinking was found to improve fiber-hydrogel bonding (See Results), a second control group of alginate blocks were printed using the same setup and were incubated in a 1% w/v EDC and 0.25% w/v NHS solution at room temperature for 24 h. For the fiber reinforced group, each sample was printed as described above so that 4 equally spaced ELAC fibers were embedded in the mid-plane of an alginate block and incubated in a 1% w/v EDC and 0.25% w/v NHS solution at room temperature for 24 h. Tensile testing of the samples was conducted using an electromechanical universal testing system with a Biobath chamber and 50 N load cell (Criterion, MTS), with 0.1% CaCl2 bath solution, at a rate of 10 mm/min until failure. The influence of fixture flotation force changes was eliminated as explained in the pull-out testing section. For each sample, the maximum calculated tensile stress was referred to as the ultimate tensile strength. The tensile modulus was calculated from the slope of the linear region of the stress-strain curves from 20% to 90% of the maximum stress value.

Three-point Bending Testing

Three-point bending testing with fixed-end beams was performed to showcase the reinforcement effect of fiber embedding on the load-bearing capacity of 3D printed hydrogels. The baseline sample was prepared by 3D printing an alginate beam (15 × 3 × 4 mm, width × height × thickness) using the FRESH process and incubating in a 1.0% w/v EDC, 0.25% NHS solution for 24 h prior. The fiber reinforced sample was an alginate beam (15 × 3

× 4 mm, width × height × thickness) with two equally spaced ELAC fiber embedded on the mid-plane, fabricated using the fiber-embedded hydrogel 3D printing process. Prior to testing, each sample was removed from the incubation fluid, blotted with lint-free Kimwipes tissues (Kimtech) and the two ends were glue bonded to two rigid sidewalls that were fixed to the platform of the MTS. Three-point bending tests were performed by using a load anvil connected to the 50 N load cell to compress the sample in the sample height direction at a rate of 10 mm/min for 3 mm.

Statistical Analysis

Data were reported as mean ± standard deviation. The pull-out force, ultimate tensile strength, and tensile modulus of different groups were analyzed using the non-parametric Kruskal-Wallis test in Minitab 18 (Minitab) with the significance level set as $p < 0.05$. An official Minitab macro, KrusMC, was used to perform non-parametric post hoc multiple pairwise comparisons.

Results and Discussion

Continuous Fiber Extruder Enables Long-fiber Embedded Hydrogel 3D Printing

We designed and implemented a low-cost fiber extruder prototype that is compatible with open-source hydrogel 3D printing hardware and software (Fig. 1A). The resulting multi-head printing platform enables the LFE-FRESH process where long fibers with desired properties, e.g., high ultimate tensile strength, are embedded into FRESH printed hydrogels. The fiber extruding mechanism was designed to be non-slip, soft, and compliant so that it can work with fibers of different sizes. A NEMA-17 stepper motor was used to actuate the extruding mechanism, which is commonly used for motion control in open-source 3D printers and can

be controlled by the same open-source software that operates the 3D printer.

The nature of the long fiber embedding process requires candidate fibers that are stiff enough for given design constraints, e.g., fiber diameter and hydrogel material properties. The fibers used in this process have a high slenderness ratio ($\geq$200) and are prone to buckling under compression. However, they must remain stable to prevent buckling while being pushed into 3D printed hydrogels. Otherwise, buckled fibers can further deform, clog the fiber guiding tube, escape from the extruding mechanism and eventually lead to embedding failure, which was observed in experiments and agreed with simulation results (Fig. 2A,C) (Simulation details can be found in the Supporting Information of this manuscript). To facilitate fiber material selection, we modeled the fiber buckling process using Euler's critical load equation and provided a design diagram for fiber printability as a function of fiber diameter and the ratio between fiber tensile modulus and bioink strength (Fig. 2B). This diagram facilitates fiber selection for LFE-FRESH because it provides a theoretical lower bound of Young's modulus of printable fibers: a fiber with Young's modulus and diameter that place itself above the lower bound may be printable. Experimental validation of the design diagram was performed using 14 fibers that were printable (Fig. 2B, green check-marks) and non-printable (Fig. 2B, red cross-marks). Details on fiber Young's modulus and bioink yield strength measurements can be found in the Supporting Information of this manuscript.

Multi-head Printing Process Preserves Geometric Fidelity of Embedded Fiber

The geometry of embedded fibers may differ from the input geometry during the embedding process and should be quantified to evaluate the printing quality. To quantitatively gauge the geometric deviation of the embedded fiber from the input geometry a 3D printed alginate block with an embedded S-shaped TiO2-doped ELAC fiber was imaged using optical coherence tomography (OCT). Imaging revealed that the fiber was successfully embedded

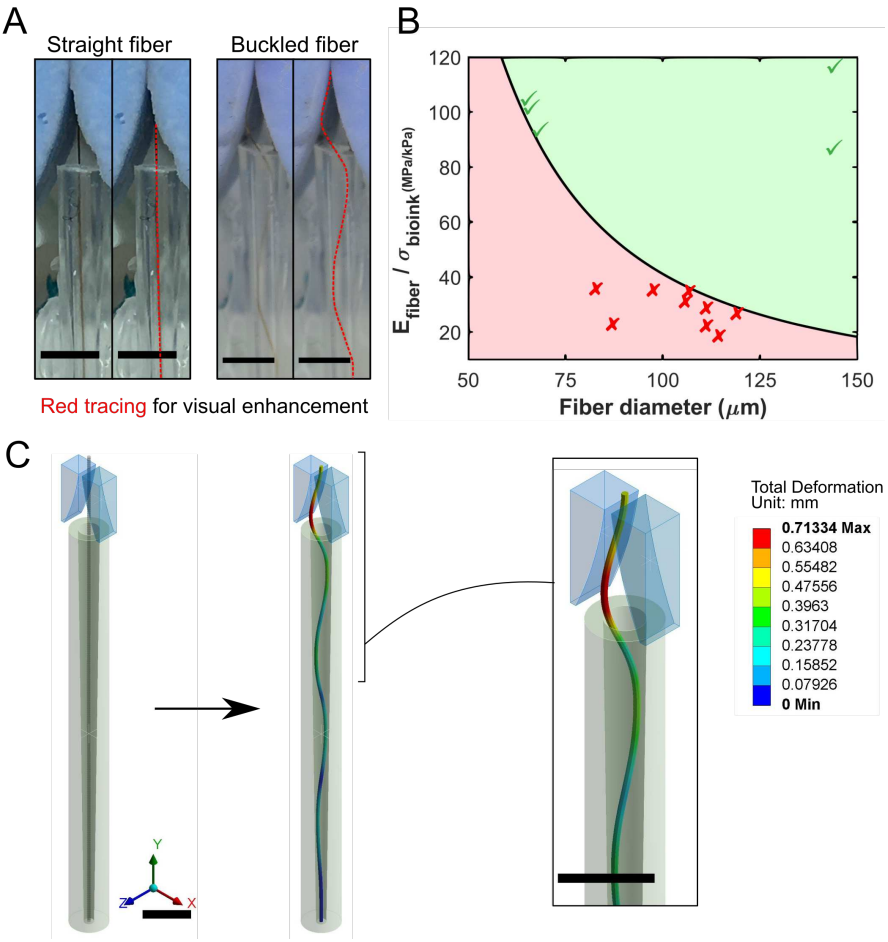

Figure 2: Fiber printability analysis (A) Photos of a fiber remaining straight while being driven by the fiber extruder (left) and a buckled fiber (right). Red tracings were added to a copy of the original photo for visual enhancement. (B) Design diagram for fiber printability as a function of fiber diameter and fiber tensile modulus v.s. bioink strength ratio. Green and red regions represent compatible and incompatible fiber properties respectively, with a curve representing the theoretical bound separating the two regions. Green check-marks and red cross-marks denote measurements of actual fibers that are compatible and incompatible with embedding for validation. (C) Simulated post-buckling fiber deformation using ANSYS with an inset showing a zoomed view. The model provides a computational tool for fiber behavior prediction and extruding mechanism design optimization. Scale bars are 2 mm

within the host alginate structure (Fig. 3). Further analysis of the deviation of embedded fiber from input geometry shows a maximum absolute displacement of 0.405 mm and a mean absolute displacement of 0.126 ± 0.067 mm (Fig. 3D). One of the contributing factors of the presented error is a small clearance between the fiber surface and the inner surface of the guiding tube, which induced a discrepancy between guiding tube trajectory and fiber geometry. Currently, the fiber guiding tube is made of a modified 10 μL pipette tip (SuperSlik, VWR) with an inner diameter of 390 μm. Using fiber guiding tubes with a smaller inner diameter, e.g., pre-pulled glass pipette tips, would further reduce the fiber-tube clearance and potentially reduce the aforementioned discrepancy.

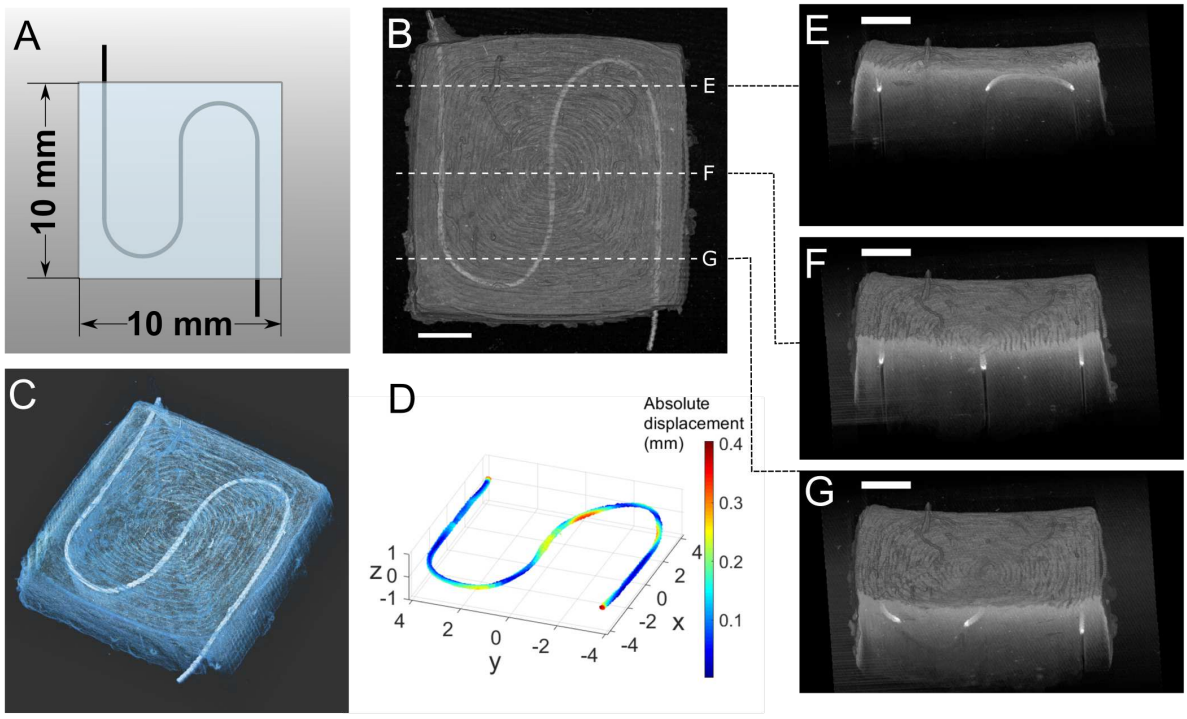

Figure 3: Geometric fidelity analysis of embedded fiber. (A) CAD model and (B) OCT image (projected view) of 3D printed alginate with embedded S-shaped feature using TiO2-doped ELAC fiber. (C) 3D reconstruction showing TiO2-doped ELAC fiber embedded in the 3D printed alginate. (D) Quantitative assessment of embedded fiber deviation from the input geometry in (A) using absolute displacement. (E-G) Sliced views of the fiber embedded alginate at different depths with dashed lines representing the corresponding positions of the slices in (B). Scale bars are 2 mm

Fiber Embedding Provides Structural Reinforcement to FRESH Printed Alginate Structures

One of the motivations of LFE-FRESH is to improve the mechanical properties of 3D printed hydrogels, e.g., alginate, using embedded fibers. To assess the reinforcement effect of fiber embedding, mechanical testing was performed to measure pull-out force, tensile modulus, and ultimate tensile strength. Pull-out testing was performed to measure the bonding strength between the hydrogel and the embedded fibers with and without-crosslinking treatments. The pull-out force of crosslinked samples was significantly higher than that of the uncrosslinked samples (Uncrosslinked: 5.380 ± 0.184 mN. Crosslinked: 26.265 ± 8.463 mN, $p < 0.05$. Fig. 4C). Additionally, to demonstrate the reinforcement effect of fiber embedding, tensile testing was performed on three groups of samples: **Baseline** - 3D printed alginate blocks without fiber embedding or crosslinking treatment, **Crosslinked** - Baseline samples with additional crosslinking treatment, and **Fiber reinforced** - Baseline samples with 4 embedded fibers and crosslinking treatment to ensure fiber-alginate bonding (Fig. 5A). The fiber reinforced group exhibited significantly higher ultimate tensile strength and tensile modulus than both the baseline and crosslinked groups, indicating that fiber embedding significantly improved the mechanical properties of 3D printed alginate (Fig. 5B-D).

Having demonstrated the reinforcement effect of fiber embedding when samples are fully hydrated, we next aimed to showcase the performance of fiber embedding when the samples were partially dehydrated, e.g., exposed to non-aqueous environments. We performed three-point bending testing on 3D printed alginate beams with and without fiber reinforcement in air and, as expected, fiber reinforcement improved load-bearing capacity (Fig. 5E,F). During the aforementioned fabrication processes, two types of biomaterials (sodium alginate and ELAC fibers) were used for fiber-reinforced alginate structure construction. Previous studies demonstrate that ELAC fibers[41] and sodium alginate bioink[40] are biocompatible and they remain biocompatible after EDC+NHS treatment.[51]

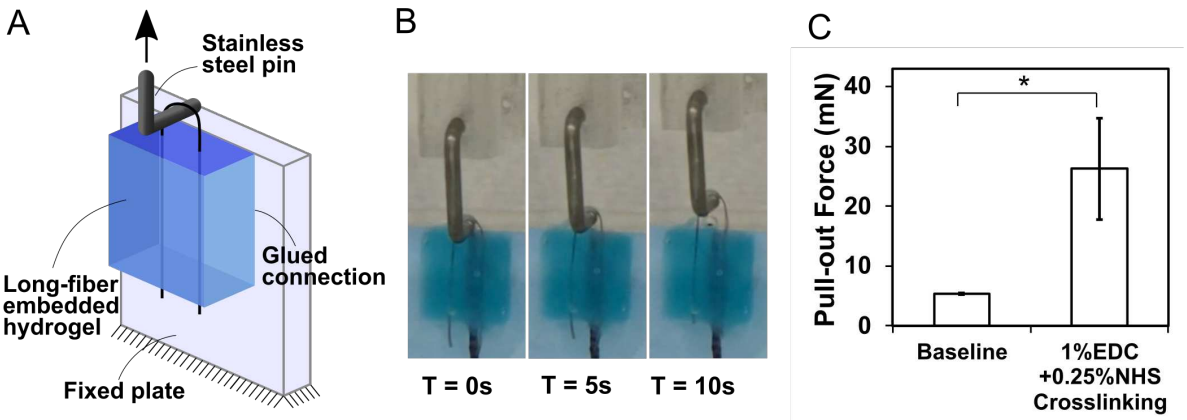

Figure 4: EDC+NHS crosslinking improves bonding between embedded fiber and 3D printed alginate. (A) Schematic drawing and (B) time-series photos of the pull-out force testing. (C) Pull-out force comparison between the baseline samples and samples treated with 1.0% w/v EDC and 0.25% w/v NHS crosslinking for 24 hr at room temperature. Asterisks represent statistically significant differences in Pull-out Force between groups ($p < 0.05$)

Versatility and Potential Applications of Long-fiber Embedded Hydrogel 3D Printing

To demonstrate the versatility of LFE-FRESH, we next used it to fabricate fiber embedded 3D printed hydrogels with a range of embedding patterns, fiber types, and hydrogel types. LFE-FRESH can print with fibers of different sizes and material types. Using the same input pattern (Fig. 6A) alginate samples were fabricated with embedded U-shaped fibers made of ELAC (Fig. 6B), Gallium-Indium-alginate mixture (Fig. 6C), polyester (Fig. 6D), silk (Fig. 6E), and stainless steel (Fig. 6F), as well as 3D printed with collagen and embedded ELAC fiber (Fig. 6G). Some of the fibers have additional properties, e.g., the electrical conductivity of stainless steel and eGaIn-alginate fibers, and may enable additional functions to 3D printed alginate components, such as soft strain sensors based on eGaIn-alginate fiber embedded alginate components. Future studies are needed to assess the biocompatibility of eGaln-embedded fibers; However, promising demonstrations of biocompatible eGaln-doped materials have been reported in the literature.[45–47] In addition to the single-fiber extrusion shown above, we also fabricated 3D printed alginate with high embedding density by simultaneously extruding three fibers (Fig. 6H).

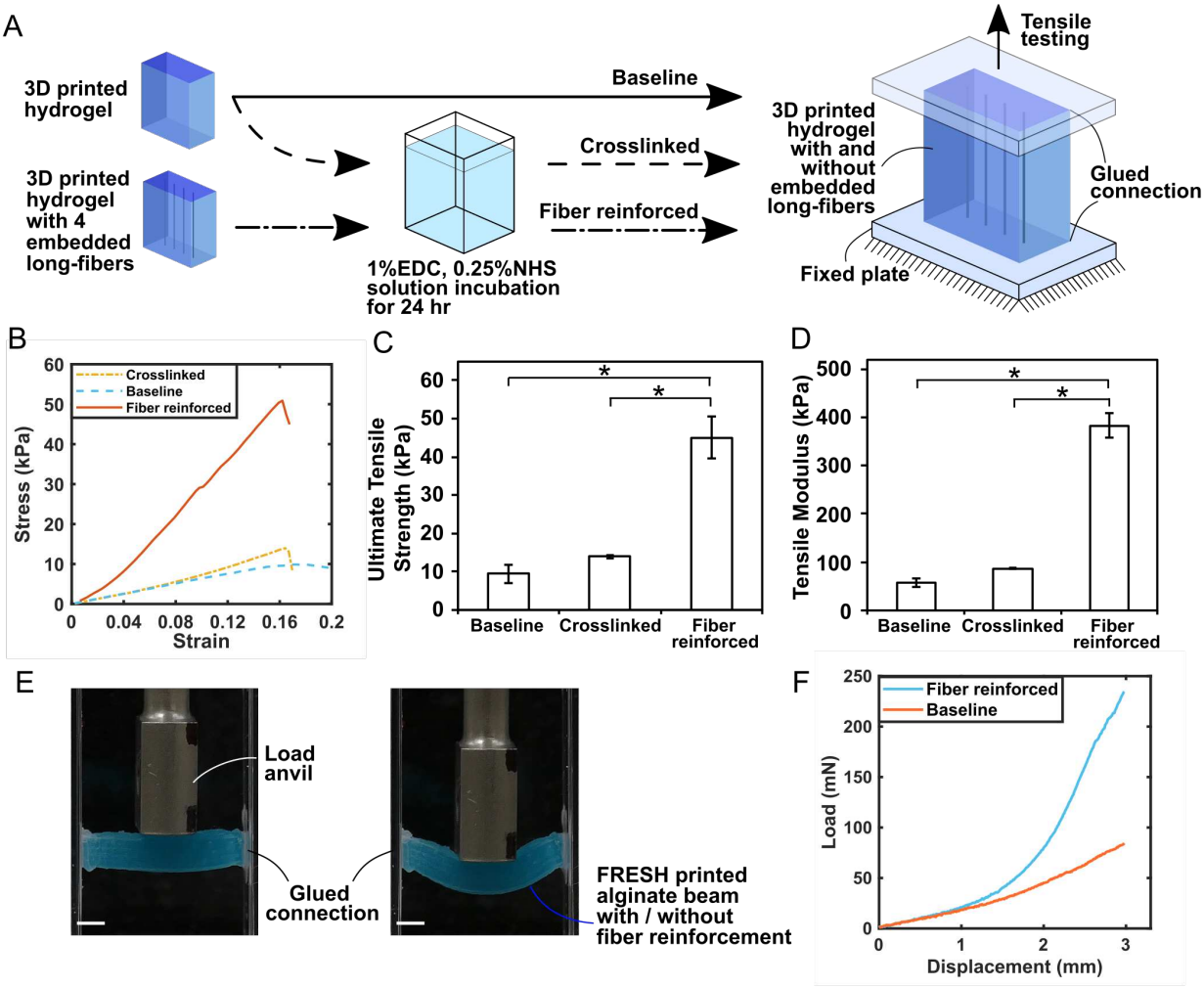

Figure 5: Long-fiber embedding provides structural reinforcement to 3D printed hydrogels. (A) Schematic drawing of tensile testing pipeline of 3D printed hydrogels with three treatments. **Baseline**: 3D printed hydrogel without treatment. **Crosslinking**: baseline subjected to 1% w/v EDC, 0.25% w/v NHS incubation for 24hr. **Fiber reinforced**: 3D printed hydrogel with 4 embedded long-fibers, subjected to 1% w/v EDC, 0.25% w/v NHS incubation for 24hr. (B) Representative stress v.s. strain curves during tensile testing for the three groups. Comparisons of (C) ultimate tensile strength and (D) tensile modulus of each treatment group, asterisks represent statistically significant differences between groups ($p < 0.05$). (E) Photos of the three-point bending testing setup. (F) Load v.s. displacement curve of the baseline and fiber reinforced samples

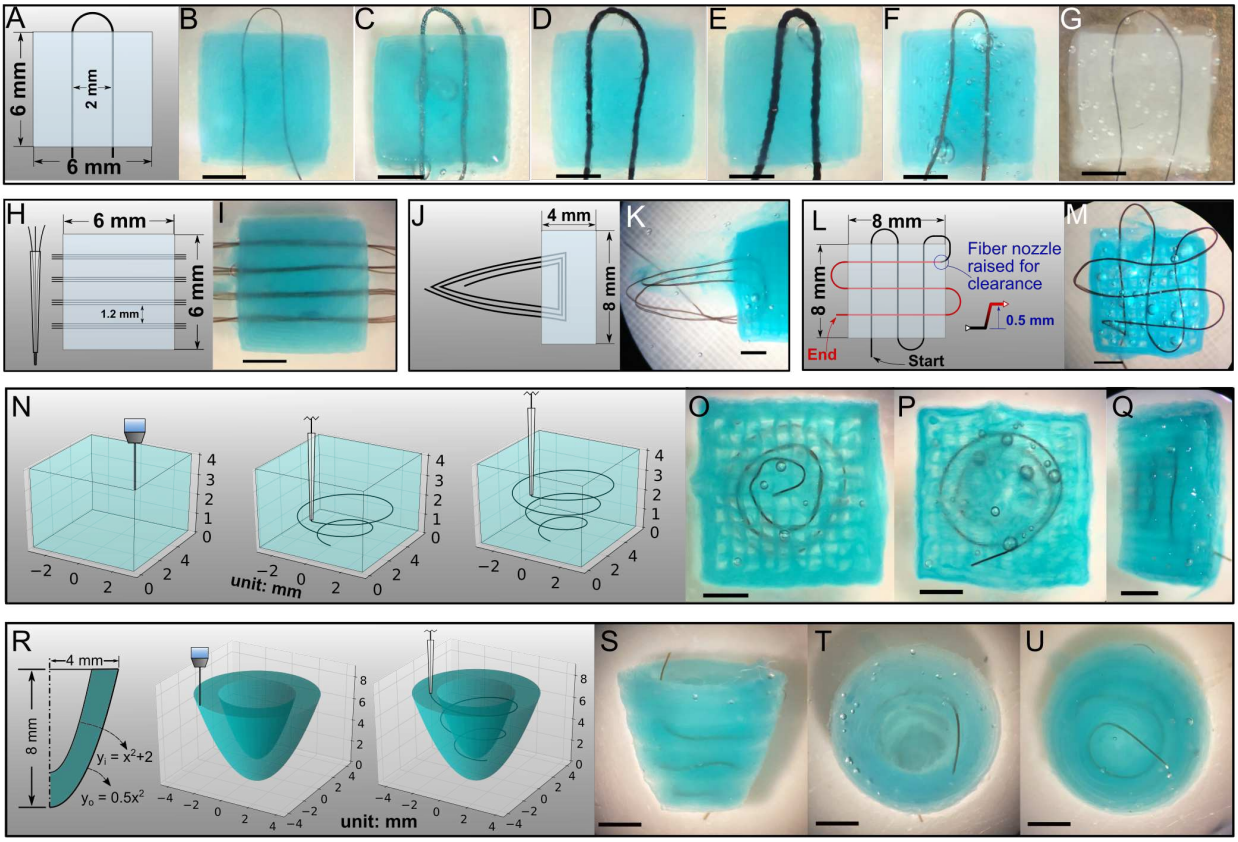

Figure 6: The multi-head printing platform is compatible with a wide range of fiber types and embedding patterns with potential applications in embedding functional fibers into 3D printed hydrogel components. (A) CAD model of hydrogel with an embedded U-shaped fiber, implemented using alginate ink with embedded long-fibers made of (B) ELAC, (C) Gallium-Indium-alginate mixture, (D) polyester, (E) silk, and (F) stainless steel, as well as (G) collagen ink with an embedded ELAC fiber. (H) CAD model and (I) implementation of 3D printed alginate embedded with 4 bundles of ELAC fibers, each of which consisted of three fibers extruded simultaneously. (J) CAD model and (K) implementation of ELAC fiber-embedded 3D printed alginate, inspired by muscle-tendon interface. (L) CAD model and (M) implementation of 3D printed alginate embedded with a 2D web-shaped feature using ELAC fiber. The fiber trace in the CAD model is color-coded to indicate different embedding depths for clearance at fiber crosspoints. (N) Schematic drawing of fabrication process of 3D printed alginate embedded with a 3D spiral-shaped helical feature using ELAC fiber, with (O) bottom, (P) top, and (Q) side views. (R) Drawing of the cross-sectional geometry of a heart sleeve model and schematic drawing of the fabrication process of a 3D printed alginate heart sleeve with embedded ELAC fiber, with (S) front, (T) top, and (U) bottom views. Scale bars are 2 mm.

Next, we demonstrated the process's ability to embed fibers into more complex 2D patterns. ELAC fibers have been reported to have tunable mechanical properties close to native tendon tissues.[48,49] We designed and fabricated a 3D printed alginate block (25% infill density) with partially embedded ELAC fiber loops, inspired by muscle-tendon interfaces that may be useful for future tendon regenerative studies[52–54] (Fig. 6J,K). To demonstrate the ability to embedded fiber at different depths within 3D printed hydrogels, we embedded an ELAC fiber using a web-shaped feature into 3D printed alginate (25% infill density), where crossing fiber sections were deposited at two different depths to avoid collision (Fig. 6L, M).

In addition to the 2D fiber embedding shown earlier, 3D structures can be embedded. To demonstrate this capability, we designed and embedded a 3D conical helix feature with varying radius and constant pitch using an ELAC fiber into a 3D printed alginate block (25% infill density) (Fig. 6N-Q). In this process, the movement of the fiber nozzle disrupts the newly printed alginate, which may reduce its mechanical strength. Hence, the resolution of subsequent fiber embedding in nozzle-affected areas will likely be lower due to the reduced gel support. This is not a major concern because such secondary embedding can be avoided by optimizing the printing path to minimize overlapping paths. In the future, the impact of nozzle passage to the printed gels can be further reduced by printing self-healing hydrogels[55–57] One of the potential future applications of such 3D fiber embedding is to provide volumetric structural reinforcement (and patterns for cell attachment) in tissue engineering. To demonstrate this, we designed and implemented a 3D printed alginate structure inspired by heart sleeve models with an embedded ELAC fiber to provide circumferential support (Fig. 6R-U). The wall thickness of the heart sleeve model is between 1.32 and 2 mm. However, the LFE-FRESH technique has the potential to work with thinner wall thickness as we have also achieved fiber embedding in alginate sheets as thin as 1 mm that sustained the passage of the fiber nozzle (sheet thickness to nozzle diameter ratio = 2.18:1, Supporting Information, section S7). Such structures may have applications in the development of low-modulus, form-fitting patient specific devices such as those that support heart muscle

contraction.[58]

In summary, the LFE-FRESH process is versatile, low-cost, and compatible with open-source 3D printing software and hardware. The chemical crosslinking treatment improves fiber-gel bonding using EDC+NHS, which was adopted because EDC+NHS crosslinking has previously been used in ELAC production.[59,60] Additionally, it does not alter the color and transparency of hydrogels, which was beneficial in assessing print fidelity in this study. In addition, other types of chemical crosslinker, such as transglutaminase, which could be used in the presence of cells,[61] or genipin, could be tested with the LFE-FRESH technique in the future. While it can be used to build long-fiber embedded 3D printed hydrogel structures with a range of fiber types and sizes, hydrogel types, 2D and 3D embedding patterns, there are limitations to overcome. After embedding one fiber path, the current extruder prototype requires manual fiber cutting before part retrieval or embedding another fiber path, which incurs additional fabrication time and complexity. In addition, cutting of ELAC fibers using scissors may leave sharp edges that could potentially damage tissues when applied in tissue engineering as shown in the Supporting Information (Fig. S1), even though ELAC fibers swell and are relatively soft when hydrated.[49] This may not be a major concern because ELAC fibers were often cut to length in prior *in vivo* tissue engineering applications.[44,53,54] Addressing this limitation in future research can further broaden the embedding capabilities of this tool, potentially by adding a computer-controlled automatic laser cutter. In addition, the fiber embedding process requires navigating a fiber guiding tube in FRESH printed hydrogel. This may introduce disturbance to the host hydrogel structure, which may need examination in future research. While the biomaterials used in ELAC fiber embedded alginate and collagen are biocompatible, the biocompatibility of any new materials or printed constructs should be examined in the future. Despite the current limitations, the LFE-FRESH process provides a tool to embed functional fibers with desired properties into hydrogel structures, which opens up opportunities to modify the existing properties and enable new functions for 3D printed hydrogels.

Due to the multi-material hydrogel additive manufacturing capabilities of the LFE-FRESH technique, it may have potential applications in many tissue engineering and soft or biohybrid robotics applications. For instance, utilizing the structural reinforcement effect of fiber embedding, we have demonstrated that functional fibers can be embedded into 3D printed alginate heart sleeve models (Fig. 6R-U). Future work could apply this concept to achieve patient specific, low-modulus devices to support heart muscle contraction . Additionally, the ability to embed fibers in printed hydrogels has direct applications in musculoskeletal tissue engineering. Given the history of ELAC fibers in tendon engineering,[54] and the recent demonstrations of FRESH printed muscle,[32] our platform may enable direct printing of tendon-muscle units by embedding ELAC fibers into cell-laden, 3D printed extracellular matrix gels. The ability to print tendon-like ends in engineered muscle could improve handling, reduce stress concentrations between engineering muscle attachment points near tendon or bone, and create new tissue constructs for volumetric muscle injury repair. Furthermore, the LFE-FRESH platform has applications in the emerging field of soft and biohybrid robotics.[5,62] By embedding strain-dependent, conductive fibers into hydrogels, soft strain sensors can be achieved for monitoring the shape morphing of compliant robots. To facilitate these applications, the LFE-FRESH platform and fabrication process can be further optimized for application specific printing resolution and expanded to additional functional fibers and hydrogel materials. In addition, future comprehensive studies should be conducted to characterize and assess the biocompatibility of new materials and fiber-gel interactions during and post embedding.

Conclusion

Here we have introduced a new method of long-fiber embedded hydrogel 3D printing using a multi-head printing platform and demonstrated its capability to create user-defined 2D and 3D embedding patterns using commercially available and custom-made functional fibers

within 3D printed hydrogels. Importantly, by embedding high-strength fibers, this process provides significant structural reinforcement to the original 3D printed hydrogels and broadens the potential applications of 3D printed soft hydrogels, especially those that require high load-bearing capacity. While we have demonstrated that this process works with the alginate and collagen bioinks previously reported with the FRESH 3D printing technique, there are other hydrogels, such as fibrinogen and methacrylated hyaluronic acid, and other hydrogel additive manufacturing techniques, such as hydrogel inkjet printing with liquid support, that may be adaptable to this method. As noted earlier, the embedding flexibility of this process can be further improved by integrating a computer-controlled fiber cutter with the presented prototype. Moving forward, embedding with multiple fiber types could bring additional functionality to 3D printed hydrogels, such embedding chemical-doped fibers toward localized, controlled drug delivery and embedding conductive fibers for signal sensing and electro-stimulation. The open-source nature of the fabrication platform facilitates easy and low-cost adoption and modification of this process for new applications.

Acknowledgement

This work was supported in part by NSF DBI 2015317 as part of the NSF/CIHR/DFG/FRQ/UKRI-MRC Next Generation Networks for Neuroscience Program and by the National Science Foundation CAREER award program (grant no. ECCS-2044785), the National Institutes of Health (grant no. 1F30HL154728-01), a Carnegie Mellon University (CMU) Department of Mechanical Engineering Collaborative Fellowship, the William and Barbara Goldsmith Family Fellowship, and the CMU Mechanical Engineering Faculty Startup.

Supporting Information Available

The following files are available free of charge.

- Supporting information.pdf: Descriptive document including custom Python scripts usage, post-buckling fiber deformation simulation, fiber Young's modulus and alginate bioink yield strength, captions for supplemental movies S1, S2, and S3, light microscopy image of cut edges of ELAC fibers, reaction scheme of EDC+NHS crosslinking of alginate and collagen, and microscope image of a 3D printed thin alginate sheet with embedded ELAC fiber

- Movie S1: The LFE-FRESH printing process

- Movie S2: Slicing through a reconstructed 3D model of a 3D printed alginate block with S-shaped fiber embedding

- Movie S3: Handling a 3D printed alginate heart sleeve with embedded electrochemically aligned collagen fiber in 0.1 percent w/v Calcium chloride solution

References

(1) Shi, Q.; Liu, H.; Tang, D.; Li, Y.; Li, X. J.; Xu, F. Bioactuators based on stimulus-responsive hydrogels and their emerging biomedical applications. *NPG Asia Materials* **2019**, *11*.

(2) Billiet, T.; Vandenhaute, M.; Schelfhout, J.; Van Vlierberghe, S.; Dubruel, P. A review of trends and limitations in hydrogel-rapid prototyping for tissue engineering. *Biomaterials* **2012**, *33*, 6020–6041.

(3) Li, J.; Mooney, D. J. Designing hydrogels for controlled drug delivery. *Nature Reviews Materials* **2016**, *1*.

(4) Lee, U. N.; Day, J. H.; Haack, A. J.; Bretherton, R. C.; Lu, W.; Deforest, C. A.; Theberge, A. B.; Berthier, E. Layer-by-layer fabrication of 3D hydrogel structures using open microfluidics. *Lab on a Chip* **2020**, *20*, 525–536.

(5) Webster-Wood, V. A.; Akkus, O.; Gurkan, U. A.; Chiel, H. J.; Quinn, R. D. Organismal engineering: Toward a robotic taxonomic key for devices using organic materials. *Science Robotics* **2017**, *2*, eaap9281.

(6) Sun, W.; Schaffer, S.; Dai, K.; Yao, L.; Feinberg, A. 3D Printing Hydrogel-Based Soft and Biohybrid Actuators : A Mini-Review on Fabrication Techniques , Applications , and Challenges. *Frontiers in Robotics and AI* **2021**, *8*, 1–10.

(7) Raviv, D.; Zhao, W.; McKnelly, C.; Papadopoulou, A.; Kadambi, A.; Shi, B.; Hirsch, S.; Dikovsky, D.; Zyracki, M.; Olguin, C.; Raskar, R.; Tibbits, S. Active printed materials for complex self-evolving deformations. *Scientific Reports* **2014**, *4*, 1–9.

(8) Xiong, Z.; Zheng, M. L.; Dong, X. Z.; Chen, W. Q.; Jin, F.; Zhao, Z. S.; Duan, X. M. Asymmetric microstructure of hydrogel: Two-photon microfabrication and stimuli-responsive behavior. *Soft Matter* **2011**, *7*, 10353–10359.

(9) Xing, J. F.; Zheng, M. L.; Duan, X. M. Two-photon polymerization microfabrication of hydrogels: an advanced 3D printing technology for tissue engineering and drug delivery. *Chemical Society Reviews* **2015**, *44*, 5031–5039.

(10) Ovsianikov, A.; Gruene, M.; Pflaum, M.; Koch, L.; Maiorana, F.; Wilhelmi, M.; Haverich, A.; Chichkov, B. Laser printing of cells into 3D scaffolds. *Biofabrication* **2010**, *2*.

(11) Cvetkovic, C.; Raman, R.; Chan, V.; Williams, B. J.; Tolish, M.; Bajaj, P.; Sakar, M. S.; Asada, H. H.; Saif, M. T. A.; Bashir, R. Three-dimensionally printed biological machines powered by skeletal muscle. *Proceedings of the National Academy of Sciences* **2014**, *111*, 10125–10130.

(12) Odent, J.; Vanderstappen, S.; Toncheva, A.; Pichon, E.; Wallin, T. J.; Wang, K.; Shepherd, R. F.; Dubois, P.; Raquez, J. M. Hierarchical chemomechanical encoding of

multi-responsive hydrogel actuators: Via 3D printing. *Journal of Materials Chemistry A* **2019**, *7*, 15395–15403.

(13) Soman, P.; Chung, P. H.; Zhang, A. P.; Chen, S. Digital microfabrication of user-defined 3D microstructures in cell-laden hydrogels. *Biotechnology and Bioengineering* **2013**, *110*, 3038–3047.

(14) Tyagi, M.; Spinks, G. M.; Jager, E. W. Fully 3D printed soft microactuators for soft microrobotics. *Smart Materials and Structures* **2020**, *29*.

(15) Gladman, A. S.; Matsumoto, E. A.; Nuzzo, R. G.; Mahadevan, L.; Lewis, J. A. Biomimetic 4D printing. *Nature Materials* **2016**, *15*, 413–418.

(16) Cheng, Y.; Chan, K. H.; Wang, X. Q.; Ding, T.; Li, T.; Lu, X.; Ho, G. W. Direct-Ink-Write 3D Printing of Hydrogels into Biomimetic Soft Robots. *ACS Nano* **2019**, *13*, 13176–13184.

(17) Bhattacharjee, T.; Zehnder, S. M.; Rowe, K. G.; Jain, S.; Nixon, R. M.; Sawyer, W. G.; Angelini, T. E. Writing in the granular gel medium. *Science Advances* **2015**, *1*, 4–10.

(18) Leblanc, K. J.; Niemi, S. R.; Bennett, A. I.; Harris, K. L.; Schulze, K. D.; Sawyer, W. G.; Taylor, C.; Angelini, T. E. Stability of High Speed 3D Printing in Liquid-Like Solids. *ACS Biomaterials Science and Engineering* **2016**, *2*, 1796–1799.

(19) Zhao, J.; Hussain, M.; Wang, M.; Li, Z.; He, N. Embedded 3D printing of multi-internal surfaces of hydrogels. *Additive Manufacturing* **2020**, *32*, 101097.

(20) Molley, T. G.; Jalandhra, G. K.; Nemec, S. R.; Tiffany, A. S.; Patkunarajah, A.; Poole, K.; Harley, B. A.; Hung, T. T.; Kilian, K. A. Heterotypic tumor models through freeform printing into photostabilized granular microgels. *Biomaterials Science* **2021**, *9*, 4496–4509.

(21) Jin, Y.; Compaan, A.; Bhattacharjee, T.; Huang, Y. Granular gel support-enabled extrusion of three-dimensional alginate and cellular structures. *Biofabrication* **2016**, *8*.

(22) Zhang, Y.; Ellison, S. T.; Duraivel, S.; Morley, C. D.; Taylor, C. R.; Angelini, T. E. 3D printed collagen structures at low concentrations supported by jammed microgels. *Bioprinting* **2021**, *21*, e00121.

(23) Bhattacharjee, T.; Gil, C. J.; Marshall, S. L.; Urueña, J. M.; O'Bryan, C. S.; Carstens, M.; Keselowsky, B.; Palmer, G. D.; Ghivizzani, S.; Gibbs, C. P.; Sawyer, W. G.; Angelini, T. E. Liquid-like Solids Support Cells in 3D. *ACS Biomaterials Science and Engineering* **2016**, *2*, 1787–1795.

(24) Hinton, T. J.; Hudson, A.; Pusch, K.; Lee, A.; Feinberg, A. W. 3D Printing PDMS Elastomer in a Hydrophilic Support Bath via Freeform Reversible Embedding. *ACS Biomaterials Science and Engineering* **2016**, *2*, 1781–1786.

(25) Hajash, K.; Sparrman, B.; Guberan, C.; Laucks, J.; Tibbits, S. Large-scale rapid liquid printing. *3D Printing and Additive Manufacturing* **2017**, *4*, 123–131.

(26) Senior, J. J.; Cooke, M. E.; Grover, L. M.; Smith, A. M. Fabrication of Complex Hydrogel Structures Using Suspended Layer Additive Manufacturing (SLAM). *Advanced Functional Materials* **2019**, *29*, 1–10.

(27) Moxon, S. R.; Cooke, M. E.; Cox, S. C.; Snow, M.; Jeys, L.; Jones, S. W.; Smith, A. M.; Grover, L. M. Suspended Manufacture of Biological Structures. *Advanced Materials* **2017**, *29*.

(28) Compaan, A. M.; Song, K.; Huang, Y. Gellan Fluid Gel as a Versatile Support Bath Material for Fluid Extrusion Bioprinting. *ACS Applied Materials and Interfaces* **2019**,

(29) Jeon, O.; Lee, Y. B.; Jeong, H.; Lee, S. J.; Wells, D.; Alsberg, E. Individual cell-

only bioink and photocurable supporting medium for 3D printing and generation of engineered tissues with complex geometries. *Materials Horizons* **2019**, *6*, 1625–1631.

(30) Hinton, T. J.; Jallerat, Q.; Palchesko, R. N.; Park, J. H.; Grodzicki, M. S.; Shue, H.-J.; Ramadan, M. H.; Hudson, A. R.; Feinberg, A. W. Three-dimensional printing of complex biological structures by freeform reversible embedding of suspended hydrogels. *Science Advances* **2015**, *1*, 1–10.

(31) Mirdamadi, E.; Tashman, J. W.; Shiwarski, D. J.; Palchesko, R. N.; Feinberg, A. W. FRESH 3D bioprinting a full-size model of the human heart. *ACS Biomaterials Science and Engineering* **2020**, 0–6.

(32) Lee, A.; Hudson, A. R.; Shiwarski, D. J.; Tashman, J. W.; Hinton, T. J.; Yerneni, S.; Bliley, J. M.; Campbell, P. G.; Feinberg, A. W. 3D bioprinting of collagen to rebuild components of the human heart. *Science* **2019**, *365*, 482–487.

(33) Bova, L.; Billi, F.; Cimetta, E. Mini-review: advances in 3D bioprinting of vascularized constructs. *Biology Direct* **2020**, *15*, 1–5.

(34) Zhao, J.; He, N. A mini-review of embedded 3D printing: Supporting media and strategies. *Journal of Materials Chemistry B* **2020**, *8*, 10474–10486.

(35) Yi, F. L.; Meng, F. C.; Li, Y. Q.; Huang, P.; Hu, N.; Liao, K.; Fu, S. Y. Highly stretchable CNT Fiber/PAAm hydrogel composite simultaneously serving as strain sensor and supercapacitor. *Composites Part B: Engineering* **2020**, *198*, 108246.

(36) Trindade, E. C.; Antônio, R. V.; Brandes, R.; de Souza, L.; Neto, G.; Vargas, V. M.; Carminatti, C. A.; de Oliveira Souza Recouvreux, D. Carbon fiber-embedded bacterial cellulose/polyaniline nanocomposite with tailored for microbial fuel cells electrode. *Journal of Applied Polymer Science* **2020**, *137*, 1–9.

(37) Tseng, H.; Puperi, D. S.; Kim, E. J.; Ayoub, S.; Shah, J. V.; Cuchiara, M. L.; West, J. L.; Grande-Allen, K. J. Anisotropic poly(ethylene glycol)/polycaprolactone hydrogel-fiber composites for heart valve tissue engineering. *Tissue Engineering - Part A* **2014**, *20*, 2634–2645.

(38) Hobzova, R.; Hrib, J.; Sirc, J.; Karpushkin, E.; Michalek, J.; Janouskova, O.; Gatenholm, P. Embedding of Bacterial Cellulose Nanofibers within PHEMA Hydrogel Matrices: Tunable Stiffness Composites with Potential for Biomedical Applications. *Journal of Nanomaterials* **2018**, *2018*.

(39) de Ruijter, M.; Hrynevich, A.; Haigh, J. N.; Hochleitner, G.; Castilho, M.; Groll, J.; Malda, J.; Dalton, P. D. Out-of-Plane 3D-Printed Microfibers Improve the Shear Properties of Hydrogel Composites. *Small* **2018**, *14*, 1–6.

(40) Khalil, S.; Sun, W. Bioprinting endothelial cells with alginate for 3D tissue constructs. *Journal of Biomechanical Engineering* **2009**, *131*, 1–8.

(41) Cheng, X.; Gurkan, U. A.; Dehen, C. J.; Tate, M. P.; Hillhouse, H. W.; Simpson, G. J.; Akkus, O. An electrochemical fabrication process for the assembly of anisotropically oriented collagen bundles. *Biomaterials* **2008**, *29*, 3278–3288.

(42) Seo, J. W.; Kim, H.; Kim, K. H.; Choi, S. Q.; Lee, H. J. Calcium-Modified Silk as a Biocompatible and Strong Adhesive for Epidermal Electronics. *Advanced Functional Materials* **2018**, *28*, 1–13.

(43) Sittinger, M.; Reitzel, D.; Dauner, M.; Hierlemann, H.; Hammer, C.; Kastenbauer, E.; Planck, H.; Burmester, G. R.; Bujia, J. Resorbable polyesters in cartilage engineering: Affinity and biocompatibility of polymer fiber structures to chondrocytes. *Journal of Biomedical Materials Research* **1996**, *33*, 57–63.

(44) Kishore, V.; Uquillas, J. A.; Dubikovsky, A.; Alshehabat, M. A.; Snyder, P. W.; Breur, G. J.; Akkus, O. In vivo response to electrochemically aligned collagen bioscaf-

folds. *Journal of Biomedical Materials Research - Part B Applied Biomaterials* **2012**, *100 B*, 400–408.

(45) Ma, Z.; Huang, Q.; Xu, Q.; Zhuang, Q.; Zhao, X.; Yang, Y.; Qiu, H.; Yang, Z.; Wang, C.; Chai, Y.; Zheng, Z. Permeable superelastic liquid-metal fibre mat enables biocompatible and monolithic stretchable electronics. *Nature Materials* **2021**, *20*, 859–868.

(46) Li, X.; Li, M.; Zong, L.; Wu, X.; You, J.; Du, P.; Li, C. Liquid Metal Droplets Wrapped with Polysaccharide Microgel as Biocompatible Aqueous Ink for Flexible Conductive Devices. *Advanced Functional Materials* **2018**, *28*, 1–8.

(47) Xia, N.; Li, N.; Rao, W.; Yu, J.; Wu, Q.; Tan, L.; Li, H.; Gou, L.; Liang, P.; Li, L.; Meng, X. Multifunctional and flexible ZrO2-coated EGaIn nanoparticles for photothermal therapy. *Nanoscale* **2019**, *11*, 10183–10189.

(48) Sun, W.; Paulovich, J.; Webster-Wood, V. Tuning the Mechanical and Geometric Properties of Electrochemically Aligned Collagen Threads Toward Applications in Biohybrid Robotics. *Journal of Biomechanical Engineering* **2021**, *143*.

(49) Alfredo Uquillas, J.; Kishore, V.; Akkus, O. Genipin crosslinking elevates the strength of electrochemically aligned collagen to the level of tendons. *Journal of the Mechanical Behavior of Biomedical Materials* **2012**, *15*, 176–189.

(50) Tashman, J. W.; Shiwarski, D. J.; Ruesch, A.; Lanni, F.; Kainerstorfer, M., Jana; Feinberg, A. W. In situ volumetric imaging and analysis of FRESH 3D bioprinted constructs using optical coherence tomography. *bioRxiv* **2021**, 10.1101/2021.06.30.450389.

(51) Fan, L.; Cao, M.; Gao, S.; Wang, T.; Wu, H.; Peng, M.; Zhou, X.; Nie, M. Preparation and characterization of sodium alginate modified with collagen peptides. *Carbohydrate Polymers* **2013**, *93*, 380–385.

(52) Learn, G. D.; McClellan, P. E.; Knapik, D. M.; Cumsky, J. L.; Webster-Wood, V.; Anderson, J. M.; Gillespie, R. J.; Akkus, O. Woven collagen biotextiles enable mechanically functional rotator cuff tendon regeneration during repair of segmental tendon defects in vivo. *Journal of Biomedical Materials Research - Part B Applied Biomaterials* **2019**, *107*, 1864–1876.

(53) Kishore, V.; Bullock, W.; Sun, X.; Van Dyke, W. S.; Akkus, O. Tenogenic differentiation of human MSCs induced by the topography of electrochemically aligned collagen threads. *Biomaterials* **2012**, *33*, 2137–2144.

(54) Younesi, M.; Islam, A.; Kishore, V.; Anderson, J. M.; Akkus, O. Tenogenic Induction of Human MSCs by Anisotropically Aligned Collagen Biotextiles. *Advanced Functional Materials* **2014**, 5762–5770.

(55) Wang, Y.; Chang, Q.; Zhan, R.; Xu, K.; Wang, Y.; Zhang, X.; Li, B.; Luo, G.; Xing, M.; Zhong, W. Tough but self-healing and 3D printable hydrogels for E-skin, E-noses and laser controlled actuators. *Journal of Materials Chemistry A* **2019**, *7*, 24814–24829.

(56) Zhang, H.; Xia, H.; Zhao, Y. Poly(vinyl alcohol) hydrogel can autonomously self-heal. *ACS Macro Letters* **2012**, *1*, 1233–1236.

(57) Taylor, D. L.; in het Panhuis, M. Self-Healing Hydrogels. *Advanced Materials* **2016**, *28*, 9060–9093.

(58) Roche, E. T.; Horvath, M. A.; Wamala, I.; Alazmani, A.; Song, S. E.; Whyte, W.; Machaidze, Z.; Payne, C. J.; Weaver, J. C.; Fishbein, G.; Kuebler, J.; Vasilyev, N. V.; Mooney, D. J.; Pigula, F. A.; Walsh, C. J. Soft robotic sleeve supports heart function. *Science Translational Medicine* **2017**, *9*, 1–12.

(59) Chapin, K.; Khalifa, A.; Mbimba, T.; McClellan, P.; Anderson, J.; Novitsky, Y.; Hijaz, A.; Akkus, O. In vivo biocompatibility and time-dependent changes in mechanical

properties of woven collagen meshes: A comparison to xenograft and synthetic mid-urethral sling materials. *Journal of Biomedical Materials Research - Part B Applied Biomaterials* **2019**, *107*, 479–489.

(60) Kishore, V.; Iyer, R.; Frandsen, A.; Nguyen, T. U. In vitro characterization of electrochemically compacted collagen matrices for corneal applications. *Biomedical Materials (Bristol)* **2016**, *11*.

(61) Orban, J. M.; Wilson, L. B.; Kofroth, J. A.; El-Kurdi, M. S.; Maul, T. M.; Vorp, D. A. Crosslinking of collagen gels by transglutaminase. *Journal of Biomedical Materials Research - Part A* **2004**, *68*, 756–762.

(62) Won, P.; Ko, S. H.; Majidi, C.; Feinberg, A. W.; Webster-Wood, V. A. Biohybrid actuators for soft robotics: Challenges in scaling up. *Actuators* **2020**, *9*, 1–11.

TOC Graphic

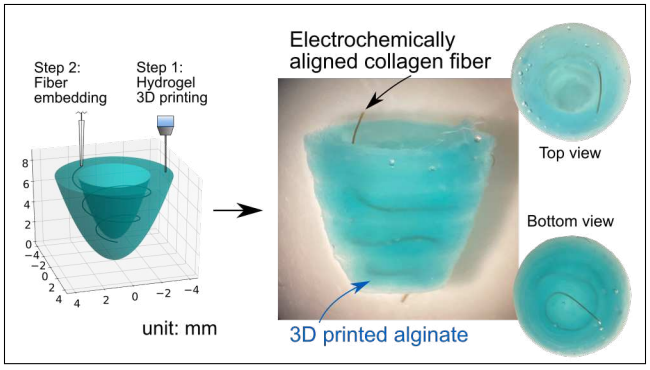

Long-fiber Embedded Hydrogel 3D Printing for Structural Reinforcement

Wenhuan Sun, Joshua W. Tashman, Daniel J. Shiwarski, Adam W. Feinberg, and Victoria A. Webster-Wood

For Table of Contents Use Only